Correction 13.08.2015

In situ Spectroscopic Study of Water Intercalation into Talc: New Features of 'Ten-Angstrom Phase' Formation

SERGEY V. RASHCHENKO[1,2,3]*, ANNA YU. LIKHACHEVA[1], SERGEY V. GORYAINOV[1], ALEXANDER S. KRYLOV[4], KONSTANTIN D. LITASOV[1,2]

[1]SOBOLEV INSTITUTE OF GEOLOGY AND MINERALOGY SB RAS, 3 KOPTYUG AVE., 630090 NOVOSIBIRSK, RUSSIA

[2]NOVOSIBIRSK STATE UNIVERSITY, 2 PIROGOV STR., 630090 NOVOSIBIRSK, RUSSIA

[3]INSTITUTE OF SOLID STATE CHEMISTRY AND MECHANOCHEMISTRY SB RAS, 18 KUTATELADZE STR., 630128 NOVOSIBIRSK, RUSSIA

[4]KIRENSKY INSTITUTE OF PHYSICS SB RAS, 50-38 AKADEMGORODOK, 660036 KRASNOYARSK, RUSSIA

*Corresponding author e-mail: rashchenko@igm.nsc.ru

ABSTRACT

The synthesis of 10 Å phase via the reaction of talc plus water at 8 GPa and 500°C was studied by in situ Raman spectroscopy using a diamond anvil cell. The initial fast (2 h) incorporation of interlayer H_2O molecules into the talc structure is traced by gradual growth of new OH stretching bands at 3592 and 3621 cm^{-1} and the shift of several framework bands. Further monitoring at H*P*-H*T* conditions over 7 h reveals gradual weakening of the 3592 cm^{-1} band, which can probably be related to the onset of the formation of 'long-run' 10 Å phase through the appearance of silanol

groups following the model proposed by Pawley et al. (American Mineralogist, vol. 95, pp. 1671–1678, 2010), influencing the interlayer hydrogen bonding.

KEYWORDS: 10 Å phase; talc; water transport; subduction

INTRODUCTION

The Earth's mantle is considered to be an important H_2O reservoir in the global water cycle where water can be stored either in hydrous phases or as defects in nominally anhydrous phases (Jacobsen and van der Lee, 2006; Kovacs et al., 2012). However, the mechanism of water transport from outer geospheres to the mantle is still debated. In cold subduction zones hydrous phases avoid dehydration and carry water to mantle depths. The serpentinized peridotite layer that lies just below the igneous oceanic crust constitutes an H_2O reservoir in the subducted lithosphere comparative in mass to the oceanic crust (Schmidt and Poli, 2014). Although serpentine dehydrates at moderate temperatures (500-700 °C), it can be a precursor for *dense hydrous magnesium silicates* (DHMS) which are stable at mantle conditions. There are three main scenarios for water behavior in serpentinized peridotite depending on the position of the subduction geotherm (Fig. 1):

1) During 'hot' subduction, the release of water from the slab basement is controlled by serpentine and then chlorite breakdown into anhydrous phases and hydrous fluid. These processes lead to the formation of the lower part of so-called double seismic zones (Dorbath et al., 2008).

2) During 'cold' subduction a direct transformation of serpentine into *phase A*, $Mg_7Si_2O_8(OH)_6$, (Ringwood and Major (1967)), is possible with almost no water fluid production (Schmidt and Poli, 2014). The retained water can then be transferred even to the lower mantle via the sequence of DHMS *phase A → phase E → superhydrous phase B → phase D(G)* (Ohtani et al., 2004).

3) As the 'normal' subduction geotherm lies above the intersection of serpentine and phase A stability curves (Fig. 1), during 'normal' subduction serpentine decomposes before phase A can be formed. However, experimental studies have shown that the so-called *ten-angstrom phase* (TAP, 10 Å phase), nominally $Mg_3Si_4O_{10}(OH)_2{\cdot}xH_2O$, can exist in the low-temperature 'dehydration gap' between the serpentine and phase A stability curves (Fig. 1). The corresponding succession of hydrous phases *serpentine → 10 Å phase → phase A*, where 10 Å phase acts as an intermediate water carrier, can retain about 25% of the initially subducted H_2O of the serpentinized peridotite even during 'normal' subduction (Schmidt and Poli, 2014).

The stability field of 10 Å phase is poorly understood. The position of the 10 Å phase dehydration curve, however, is particularly important because it limits the range of subduction geotherms where H_2O can be retained in a slab via *serpentine → 10 Å phase → phase A* transformations. According to equilibrium experiments of Pawley et al. (2011), the dehydration reaction *10 Å phase → enstatite + coesite + H_2O* occurs at 690°C at pressures below 7.5 GPa. In a number of studies 10 Å phase was obtained at higher temperatures of 700-750 °C (Yamamoto and Akimoto, 1977; Pawley and Wood, 1995; Dvir et al., 2011) – see Fig 1. The latter studies, however, were synthesis experiments and can therefore not be considered as equilibrium. Most significantly, nanoinclusions of 10 Å phase have been found in mantle olivine (Khisina and Wirth, 2008), which strongly supports the possibility of its occurrence in nature.

The structure of 10 Å phase is very similar to that of trioctahedral mica with 2:1 tetrahedral-octahedral layers parallel to (001), the interlayer space being occupied by H_2O molecules (Comodi 2005). The H_2O stoichiometry of 10 Å phase is not well constrained and varies, according to different estimations, from 0.6 to 2 H_2O molecules per formula unit (Sclar and Carrison (1966) Yamamoto and Akimoto (1977) Bauer and Sclar (1981) Wunder and Schreyer (1992)). However,

recent structural and thermodynamic studies (Comodi 2005, Pawley et al. (2010; 2011)) suggest 1 H_2O molecule per formula unit as the most probable water content.

One of the most enigmatic features of 10 Å phase is the dependence of its properties on synthesis duration, first shown by Fumagalli et al. (2001). The first interpretation assumed a gradual hydration of 10 Å phase during synthesis (Fumagalli et al., 2001) which was not confirmed by the dehydration experiments of Pawley et al. (2011). Then a model of gradual accumulation of Si vacancies in the 10 Å phase via hydrogarnet-type substitution up to the composition $Mg_3[(Si_{3.83}4H_{0.17})O_{10}](OH)_2 \cdot H_2O$ was proposed (Welch et al., 2006, Phillips et al., 2007, Pawley et al., 2010). In the case of synthesis of 10 Å phase via interaction of talc with H_2O (e.g. Chinnery et al., 1999), this model predicts a two-stage process. First, H_2O molecules enter the interlayer space of talc, expanding d_{001}. This stage was monitored in situ by Chinnery at al. (1999) by measuring energy-dispersive X-ray diffraction from the sample d_{001}, and lasts tens of minutes. Then the expanded talc structure equilibrates via accumulation of hydrogarnet-type Si vacancies. This 'maturation' process lasts hours and days and results in changes in stoichiometry, H-bonding scheme, and transformation of hydrophobic talc layers into hydrophilic layers of 10 Å phase. The understanding of the 'maturation' of 10 Å phase is crucial for correct comparison of 'short-' and 'long-run' experimental data, and for correct estimation of 10 Å phase water content, important for petrological implications.

A detailed study of the complex two-stage formation of 10 Å phase requires application of in situ techniques instead of quenching experiments widely used in previous investigations. The only in situ study of 10 Å phase formation is the experiment of Chinnery at al. (1999), where the shift of the basal diffraction peak indicating water intercalation into talc was measured. However, this method could not reveal the details of 10 Å phase 'maturation' because the latter is not associated with significant changes in d_{001}. Since the structural model of 10 Å phase proposed by Phillips et al. (2007) implies that the changes in water bonding occur during 'maturation', we have used the OH-

92 stretching Raman bands to monitor in situ the reaction and follow both steps. Here we present the
93 results of an in situ Raman study of 10 Å phase formation via the reaction of talc with water at 8
94 GPa and 500°C and subsequent quenching using the diamond anvil cell technique. Special emphasis
95 is placed on the behavior of water constituents and possible role of Si vacancies.

96

97 **EXPERIMENTAL**

98 The most convenient way to obtain pure 10 Å phase is the reaction '*talc* + $H_2O \rightarrow$ *10 Å phase*'
99 (*e.g.* Chinnery et al., 1999). A natural sample of talc from Shabrovskoye deposit (Central Ural) with
100 $Mg_{2.94}Fe_{0.05}Al_{0.05}Si_{3.97}O_{10}(OH)_2$ stoichiometry (by X-ray fluorescence analysis) was used as a
101 starting material; similar samples with about 1% replacement of Mg by Fe and minor alumina
102 content were used for 10 Å phase synthesis by Chinnery et al. (1999) and Pawley et al. (1995,
103 2011). A Diacell μScope diamond anvil cell (EasyLab) with gas membrane and resistive heating
104 was used for in situ Raman spectroscopy. Raman spectra were collected on a LabRAM HR800
105 spectrometer (HORIBA Jobin Yvon) with 1024 pixel CCD detector using the 514.5-nm argon laser
106 (Melles Griot). An Olympus BX41 microscope with backscattering geometry was used with
107 SLMPLN 50X objective (0.37 mm working distance, 0.75 numerical aperture, 2 μm focal spot size).
108 The spectral resolution was set to ~3.0 cm^{-1} at a Raman shift of 1300 cm^{-1}. This resolution was
109 achieved by using a grating with 1800 grooves/mm and equivalent 150 μm slits and pinhole. Such
110 resolution provides the accuracy of peak position determination of about 0.5 cm^{-1}. The position, full
111 width at half maximum (FWHM) and integral intensity of Raman bands were fitted using Gaussian
112 model in the Fityk 0.9.8 program (Wojdyr, 2010).

113 Several flakes of talc up to 100 μm in diameter were placed in a 200 μm-diameter hole in an
114 Inconel gasket pre-indented to 100 μm thickness, then filled with distilled water. Two experiments
115 were performed. In the first (calibration) experiment a chip of $SrB_4O_7:Sm^{2+}$ pressure calibrant

(Rashchenko et al., 2013; 2015) was also placed in the cell. Then the sample was pressurized to 8 GPa and heated to 500°C. The temperature was measured using a type K thermocouple in contact with the gasket and diamond anvil. At these conditions, the positions of the main lattice bands of talc were recorded for future reference. The second experiment was performed without pressure calibrant to avoid dissolution of $SrB_4O_7:Sm^{2+}$ in the fluid. The talc spectrum collected previously at 8 GPa / 500°C was used as a reference to reach the same high-pressure / high-temperature (H*P*-H*T*) conditions recorded with the pressure calibrant. The progress of the reaction *'talc + H_2O → 10 Å phase'* was then monitored in situ for about three hours. After reaction completion (see Results), the spectrum of 10 Å phase was monitored at static H*P*-H*T* conditions for about 7 hours. Raman spectra were collected every 15-25 min in both lattice-mode (below 1250 cm^{-1}) and O-H stretching (3000-3900 cm^{-1}) regions. The resulting duration of 10 Å phase synthesis in our experiment is about 10 hours, and therefore our product can be regarded as 'short-run' 10 Å phase, in contrast to 'long-run' phase obtained after hundreds hours of synthesis (e.g. Fumagalli et al., 2001).

The quenching of synthesized 10 Å phase was performed in the following two steps. First, the sample was cooled from 500°C to room temperature over four hours. Then the sample pressure was gradually decreased from 8 to ~6 GPa, followed by abrupt decompression to ambient conditions due to the hysteretic behavior of the gas membrane. The decompression stage lasted about 3 hours. The pressure was estimated via interpolation of the O-H stretching frequencies between 8 GPa and room pressure points.

RESULTS

The starting spectrum of talc collected at ambient conditions (Fig. 2, Table 1) is similar to that reported by Fumagalli et al. (2001) for talc flakes with the (001) plane perpendicular to the optical axis. The changes in the talc spectrum upon pressure and temperature increase are shown in Figure

2. Note that the contraction of the sample hole upon pressure increase from 6 to 8 GPa slightly changed the orientation of the talc flakes, which activated the band at 181 cm^{-1} and decreased the intensity of the other bands below 250 cm^{-1}.

Soon after the conditions of 8 GPa and 500°C were achieved, the 10 Å phase began to form (Fig. 3). Since the main difference between talc and 10 Å phase is the presence of interlayer water molecules in the latter, the clearest evidence of the *talc* + H_2O → *10 Å phase* reaction progress was observed in the O-H stretching region. Two bands at 3590 and 3631 cm^{-1}, corresponding to 10 Å phase, replaced the 3681 cm^{-1} band of talc (Fig. 3b). Because of the similarity of the lattice spectra of talc and 10 Å phase, the corresponding transformation could be observed here only from the shift of the 376 cm^{-1} talc band to a 364 cm^{-1} 10 Å phase band (Fig. 3). The observed changes in the band intensities below 250 cm^{-1} are mostly related to orientation change of newly-formed 10 Å phase with respect to the initial talc flakes. According to the changes in both lattice and O-H stretching region, the reaction was complete after 120 min at 8 GPa / 500°C, in agreement with optical observation: talc flakes were substituted by a fine-grained mass of 10 Å phase (Fig. 4). A discrepancy with Chinnery et al. (1999) who observed *talc* + H_2O → *10 Å phase* transformation in 15 minutes can be attributed to the fact that we used large talc flakes up to 100 μm in diameter, whereas Chinnery et al. (1999) used a more fine-grained powder, which could contribute to faster kinetics.

The post-formation treatment of the newly-formed 10 Å phase at 8 GPa / 500°C over 7 hours shows no changes in band intensities or widths in the lattice region (Fig. 5). In contrast, a progressive broadening and slow intensity decrease was observed for the 3590 cm^{-1} band in the O-H stretching region (Fig. 6). This may indicate a slow gradual process affecting the arrangement of interlayer H_2O in the newly-formed 10 Å phase.

Upon cooling, a slight low-frequency shift was observed for the 700 and 229 cm^{-1} bands in the lattice region and for both the 3590 and 3631 cm^{-1} O-H bands (Figs. 5 and 7). Subsequent pressure decrease caused a strong low-frequency shift of the 700, 364 and 229 cm^{-1} lattice bands, whereas the band at 110 cm^{-1} was found to be insensitive to both temperature and pressure. In the O-H stretching region, an opposite shift was observed for the 3590 and 3631 cm^{-1} bands, which moved to higher and lower frequencies, respectively (Table 1).

The appearance of a band near 530 cm^{-1} during quenching (Fig. 7a) is most probably related to an orientation effect, since this band was not observed after final decompression. A broad weak band near 3650 cm^{-1}, which also appears during quenching, correlates in intensity with the band at 530 cm^{-1}, and therefore could be due to the orientation effect. However, the persistence of this band in the ambient spectrum, where it shifts to 3667 cm^{-1}, could also indicate some rearrangement of interlayer H_2O during quenching.

The spectrum of quenched 10 Å phase at ambient conditions (Fig. 7) is identical to previously reported spectra (Fumagalli et al. (2001), Comodi et al. (2006; 2007)) in both the lattice and O-H stretching regions. It is important to note an appreciable difference between the lattice spectrum of quenched and 'in-situ' 10 Å phase (Fig. 7a), obviously caused by different orientation of the grains. It is interesting that, in contrast to the lattice spectrum, the OH stretching bands are almost insensitive to orientation (Fig. 7b). This observation agrees with previous Raman measurements performed on oriented crystals (Fumagalli et al. (2001) and aggregates of non-oriented crystals (Comodi et al. (2007)), showing the same OH spectrum.

The Raman bands of talc and 10 Å phase observed at ambient conditions and at 8 GPa / 500 °C are listed in Table 1. The assignments for lattice bands of 10 Å phase are given by analogy with the talc spectrum, according to Rosasco and Blaha (1980).

DISCUSSION

The IR spectroscopic study of Parry et al. (2007) demonstrated that the talc band of structural hydroxyls near 3675 cm^{-1} remains as the main band in the spectrum of 10 Å phase as well. It is consistent with the fact that interlayer H_2O molecules in the 10 Å phase are situated far from structural hydroxyls and can hardly affect their stretching frequency. In contrast, in the Raman spectrum of 10 Å phase this band is hardly pronounced. The latter caused an erroneous assignment of another strong Raman band at 3621 cm^{-1} to structural hydroxyls (Fumagalli et al. (2001). We suppose that both bands which appear in the O-H stretching region of the 10 Å phase (3590 and 3631 cm^{-1} at 8 GPa / 500°C; 3592 and 3621 cm^{-1} at ambient conditions) are related to the O-H stretching of interlayer water molecules. The latter implies an asymmetric environment of interlayer H_2O with one proton involved into a hydrogen bond with tetrahedral layer (the lower frequency band). Another proton can be involved into a weaker hydrogen bond or remain not bonded.

The behavior of the O-H stretching bands during the experiment allows to divide the formation of the 10 Å phase into two steps. The first step is accompanied by the appearance and growth of the bands at 3590 and 3631 cm^{-1} (at 8 GPa / 500°C) and lasts about 120 minutes (Fig. 3b). We interpret this step as intercalation of water molecules into the interlayer space of talc with formation of the 'short synthesis' 10 Å phase (Fumagalli *et al.*, 2001).

The next step ('maturation') of the 10 Å phase is much slower and can be observed in situ as gradual broadening and extinction of the band at 3631 cm^{-1} (at 8 GPa / 500°C). We observed this process only for the first ten hours (Figs. 3b and 6), but, extrapolating it for a longer time, we suppose that after few hundreds of hours at 8 GPa and 500°C the band at 3631 cm^{-1} should completely disappear from the Raman spectrum of the 10 Å phase. The latter is consistent with previous observations, which demonstrated that (1) the 'short synthesis' 10 Å phase can be synthesized in few hours, whereas its transformation into the 'long synthesis' phase ('maturation')

211 requires hundreds of hours (Fumagalli *et al.*, 2001), and (2) the 'long synthesis' 10 Å phase is
212 characterized by the absence of the band at 3631 cm^{-1} at 8 GPa and 500°C (Comodi *et al.*, 2007).

213 The observed extinction of the band at 3631 cm^{-1} can be interpreted as a result of gradual
214 reorientation of the interlayer H_2O molecules. Assuming that this band is associated with H_2O
215 bonded to O-atoms of tetrahedral layer, we suppose that during 'maturation' of the 10 Å phase this
216 H-bond becomes unfavorable. The latter is consistent with the model of gradual accumulation of Si
217 vacancies during the 'maturation' of the 10 Å phase (Welch et al., 2006; Phillips et al., 2007;
218 Pawley et al., 2010) with each vacancy compensated by four OH groups: one Mg-OH and three Si-
219 OH silanol groups. The Si-OH groups in the tetrahedral layer are (1) less favorable as proton
220 acceptors than ordinary O-atoms, and (2) can serve as proton donors for interlayer H_2O. Herewith,
221 the accumulation of the silanol groups associated with Si vacancies in the tetrahedral layer should
222 change the role of interlayer H_2O from proton donors to proton acceptors, leading to the extinction
223 of the band at 3631 cm^{-1}. The fact that we did not observe any new bands related to the O-H
224 stretching of silanol groups is probably caused by very intense Raman signal of water fluid present
225 in DAC, hiding the range between 3100 and 3500 cm^{-1}.

226 The proposed model agrees well with the previous observations of the 'maturation' process of 10
227 Å phase (Fumagalli et al., 2001) and the model of Si vacancies accumulation (Pawley et al., 2010);
228 however, a number of further experiments using NMR and in situ Raman and IR techniques are
229 needed to constrain the details of 10 Å phase 'maturation' and differences between 'short' and
230 'long' synthesis samples.

231

232 **IMPLICATIONS**

The 10 Å phase plays a crucial role if the succession of hydrous phases *serpentine → 10 Å phase → phase A* is considered as a mechanism of water transport to the deep mantle. However, a wide consideration of the 10 Å phase in petrological models was hampered by a number of disputable issues concerning its possible metastability, vague water content, and dependence of properties on the synthesis duration. Our results give a new insight into the latter issue, showing that the orientation of interlayer H_2O molecules in water-intercalated talc ('short-synthesis' 10 Å phase) does change upon subsequent H*P*-H*T* treatment. The latter convincingly agrees with a model of gradual accumulation of Si vacancies during synthesis of the 10 Å phase, proposed by Pawley et al. (2010).

ACKNOWLEDGEMENTS

This research was performed within the project *"The formation mechanisms and stability of hydrous high-pressure silicates in MgO-SiO_2-H_2O system during subduction of oceanic lithosphere"* supported by Russian Foundation for Basic Research [grant #13-05-00185]. A partial support from Russian Ministry of Education and Science [grant #14.B25.31.0032] and Russian Scientific Fund [grant #14-13-00834] is acknowledged. We also acknowledge Mark D. Welch and an anonymous reviewer for a helpful revision of the manuscript.

REFERENCES

Bauer, J.F. and Sclar, C.B. (1981). The 10 Å phase in the system MgO-SiO_2-H_2O. American Mineralogist, 66, 576-585.

Chinnery, N.J., Pawley, A.R., and Clark, S.M. (1999). In situ observation of the formation of 10 Å phase from talc + H_2O at mantle pressures and temperatures. Science, 286, 940-942.

Comodi, P. (2005). The 10 Å phase: Crystal structure from single-crystal X-ray data. American Mineralogist, 90, 1012-1016.

Comodi, P., Cera, F., Dubrovinsky, L., and Nazzareni, S. (2006). The high-pressure behaviour of the 10 Å phase: A spectroscopic and diffractometric study up to 42 GPa. Earth and Planetary Science Letters, 246, 444-457.

Comodi, P., Cera, F., Nazzareni, S., and Dubrovinsky, L. (2007). Raman spectroscopy of the 10 Å phase at simultaneously HP-HT. European Journal of Mineralogy, 19, 623-629.

Dorbath, C.C., Gerbault, M., Carlier, G., and Guiraud, M. (2008). The double seismic zone of the Nazca plate in Northern Chile: High resolution velocity structure, petrological implications and thermomechanical modelling. Geochemistry Geophysics Geosystems, 9, 1-29.

Dvir, O., Pettke, T., Fumagalli, P., and Kessel, R. (2011) Fluids in the peridotite–water system up to 6 GPa and 800°C: New experimental constrains on dehydration reactions. Contributions to Mineralogy and Petrology, 161, 829-844.

Fumagalli, P. and Poli, S. (1999). Phase relationships in hydrous peridotites at high pressure: Preliminary results of multianvil experiments. Periodico di Mineralogia, 68, 275-286.

Fumagalli, P., Stixrude, L., Poli, S., and Snyder, D. (2001). The 10 Å phase: A high-pressure expandable sheet silicate stable during subduction of hydrated lithosphere. Earth and Planetary Science Letters, 186, 125-141.

Fumagalli, P. and Poli, S. (2005). Experimentally determined phase relations in hydrous peridotites to 6.5 GPa and their consequences on the dynamics of subduction zones. Journal of Petrology, 46, 555-578.

Fumagalli, P. and Stixrude, L. (2007). The 10 Å phase at high pressure by first principles calculations and implications for the petrology of subduction zones. Earth and Planetary Science Letters, 260, 212-226.

Fumagalli, P., Zanchetta, S., and Poli, S. (2009). Alkali in phlogopite and amphibole and their effects on phase relations in metasomatized peridotites: a high-pressure study. Contributions to Mineralogy and Petrology, 158, 723–737.

Jacobsen, S.D. and van der Lee, S. (eds.) (2006). Earth's deep water cycle. Washington, DC: American Geophysical Union.

Khisina, N.R. and Wirth, R. (2008). Nanoinclusions of high-pressure hydrous silicate, $Mg_3Si_4O_{10}(OH)_2 \cdot nH_2O$ (10 Å phase), in mantle olivine: Mechanisms of formation and transformation. Geochemistry International, 46, 319-327.

Khodyrev, O.Y. and Agoshkov, V.M. (1986). Phase transformations of serpentine in the system $MgO\text{-}SiO_2\text{-}H_2O$ at the pressure range 40 to 80 kbar. Geokhimiya, 264-269.

Kleppe, A.K. and Jephcoat, A.P. (2006). Raman spectroscopic studies of hydrous and nominally anhydrous deep mantle phases. In: Jacobsen, S.D. and van der Lee, S. (eds.) Earth's deep water cycle. Washington, DC: American Geophysical Union, 69-93.

Kovacs, I., Green, D.H., Rosenthal, A., Hermann, J., O'Neill, H.S., Hibberson, W.O., and Udvardi, B. (2012). An experimental study of water in nominally anhydrous minerals in the upper mantle near the water-saturated solidus. Journal of Petrology, 53, 2067-2093.

Ohtani, E., Litasov, K., Hosoya, T., Kubo, T., and Kondo, T. (2004). Water transport into the deep mantle and formation of a hydrous transition zone. Physics of the Earth and Planetary Interiors, 143, 255-269.

Parry, S.A., Pawley, A.R., Jones, R.L., and Clark, S.M. (2007). An infrared spectroscopic study of the OH stretching frequencies of talc and 10 Å phase to 10 GPa. American Mineralogist, 92, 525-531.

Pawley, A.R. and Wood, B.J. (1995). The high-pressure stability of talc and 10 Å phase – potential storage sites for H_2O in subduction zones. American Mineralogist, 80, 998-1003.

Pawley, A.R., Welch, M.D., Lennie, A.R., and Jones, R.L. (2010). Volume behavior of the 10 Å phase at high pressures and temperatures, with implications for H_2O content. American Mineralogist, 95, 1671-1678.

Pawley, A.R., Chinnery, N.J., Clark, S.M., and Walter, M.J. (2011). Experimental study of the dehydration of 10 Å phase, with implications for its H_2O content and stability in subducted lithosphere. Contributions to Mineralogy and Petrology, 162, 1279-1289.

Pawley, A.R. and Welch, M.D. (2014). Further complexities of the 10 Å phase revealed by infrared spectroscopy and X-ray diffraction. American Mineralogist, 99, 712-719.

Phillips, B.L., Mason, H.E., and Guggenheim, S. (2007). Hydrogen bonded silanols in the 10 Å phase: Evidence from NMR spectroscopy. American Mineralogist, 92, 1474-1485.

Rashchenko, S.V., Likhacheva, A.Y., and Bekker, T.B. (2013). Preparation of a macrocrystalline pressure calibrant $SrB_4O_7:Sm^{2+}$ suitable for the HP-HT powder diffraction. High Pressure Research, 33, 720-724.

Rashchenko, S.V., Kurnosov, A., Dubrovinsky, L., and Litasov, K.D. (2015) Revised calibration of the $Sm:SrB_4O_7$ pressure sensor using the Sm-doped yttrium-aluminum garnet primary pressure scale Journal of Applied Physics, 117, 145902.

Ringwood, A.E. and Major, A. (1967). High-pressure reconnaissance investigations in the system Mg_2SiO_4-MgO-H_2O. Earth and Planetary Science Letters, 2, 130-133.

Sclar, C.B. and Carrison, L.C. (1966). High-pressure reactions and shear strength of serpentinized dunite. Science, 153, 1285-1286.

Schmidt, M.W. and Poli, S. (1998). Experimentally based water budgets for dehydrating slabs and consequences for arc magma generation. Earth and Planetary Science Letters, 163, 361-379.

Schmidt, M.W. and Poli, S. (2014). Devolatilization during subduction. In: Holland, H.D. and Turekian, K.K. (eds.) Treatise on Geochemistry (2nd edition). Amsterdam, Netherlands: Elsevier, 669-701.

Syracuse, E.M., van Keken, P.E., and Abers, G.A. (2010). The global range of subduction zone thermal models. Physics of the Earth and Planetary Interiors, 183, 73-90.

Ulmer, P. and Trommsdorff, V. (1995). Serpentine stability to mantle depths and subduction-related magmatism. Science, 268, 858-861.

Wang, J.W., Kalinichev, A.G., and Kirkpatrick, R.J. (2004). Molecular modeling of the 10 Å phase at subduction zone conditions. Earth and Planetary Science Letters, 222, 517-527.

Welch, M.D., Pawley, A.R., Ashbrook, S.E., Mason, H.E., and Phillips, B.L. (2006). Si vacancies in the 10 Å phase. American Mineralogist, 91, 1707-1710.

Wojdyr, M. (2010). Fityk: a general-purpose peak fitting program. Journal of Applied Crystallography, 43, 1126-1128.

Wunder, B. and Schreyer, W. (1992). Metastability of the 10 Å phase in the system MgO-SiO_2-H_2O (MSH): What about hydrous MSH phases in subduction zones? Journal of Petrology, 33, 877-889.

Yamamoto, K. and Akimoto, S. (1977). The system MgO-SiO_2-H_2O at high pressures and temperatures – stability field for hydroxylchondrodite, hydroxylclinohumite and 10 Å phase. American Journal of Science, 277, 288-312.

FIGURES CAPTIONS

Figure 1. Stability of low-temperature hydrous phases (*Serp* – serpentine, *Chl* – chlorite) in serpentinized peridotite after Schmidt and Poli (1998). The Moho geotherms in subducting slab for Antilles, New Zealand and Kermadec after Syracuse et al. (2010) are shown as examples of 'hot', 'normal' and 'cold' subduction, respectively. *P-T* conditions of experiments with 10 Å phase among run products are shown as diamonds (Yamamoto and Akimoto, 1977; Welch et al., 2006 – syntheses from oxides/hydroxides in pure MgO-SiO_2-H_2O system), triangles (Ulmer and Trommsdorff, 1995; Khodyrev and Agoshkov, 1986 – syntheses from natural serpentine), '×' (Pawley and Wood, 1995 – syntheses from natural talc), and '+' (Fumagalli and Poli, 2005; Dvir et al., 2011 – syntheses from gel with peridotite composition).

Figure 2. Raman spectra of *'talc + H_2O'* sample in the lattice-mode region collected during pressure and temperature increase from ambient conditions to 8 GPa / 500°C.

Figure 3. Raman spectra demonstrating *'talc + H_2O → 10 Å phase'* reaction process in a) lattice-mode region and b) O-H stretching region. Timing start corresponds to the achievement of 8 GPa / 500°C conditions.

Figure 4. The sample at 8 GPa / 500 °C before (*a*) and after (*b*) *'talc + H_2O → 10 Å phase'* transformation.

Figure 5. The behavior of selected Raman bands of the newly-formed 10 Å phase in the lattice-mode (up) and O-H stretching (down) regions at formation conditions (*a*), during temperature decrease (*b*), and during final decompression (*c*).

366 **Figure 6.** Evolution of selected bandwidths of newly-formed 10 Å phase at synthesis conditions
367 (*a*), during temperature decrease (*b*), and during final decompression (*c*) (frequencies in legend refer
368 to 8 GPa / 500°C conditions).

369 **Figure 7.** Raman spectra of the newly-formed 10 Å phase during temperature and pressure
370 decrease: a) – the lattice-mode region; b) – the O-H stretching region.

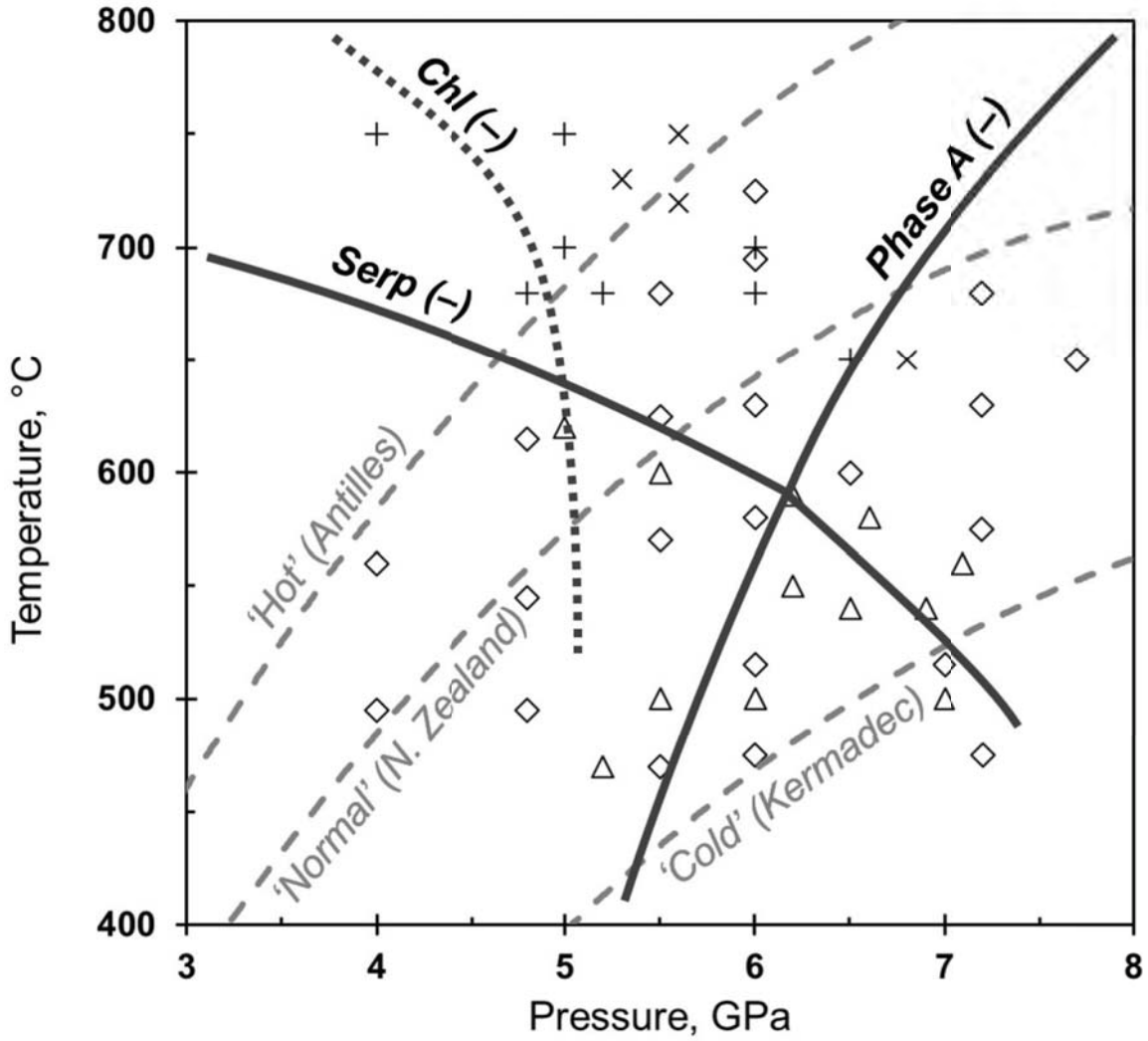
800
700
600
500
400
3
4
5
6
7
8
Temperature, °C
Pressure, GPa
Chl (–)
Serp (–)
Phase A (–)
'Hot' (Antilles)
'Normal' (N. Zealand)
'Cold' (Kermadec)

Figure 1

Figure 2

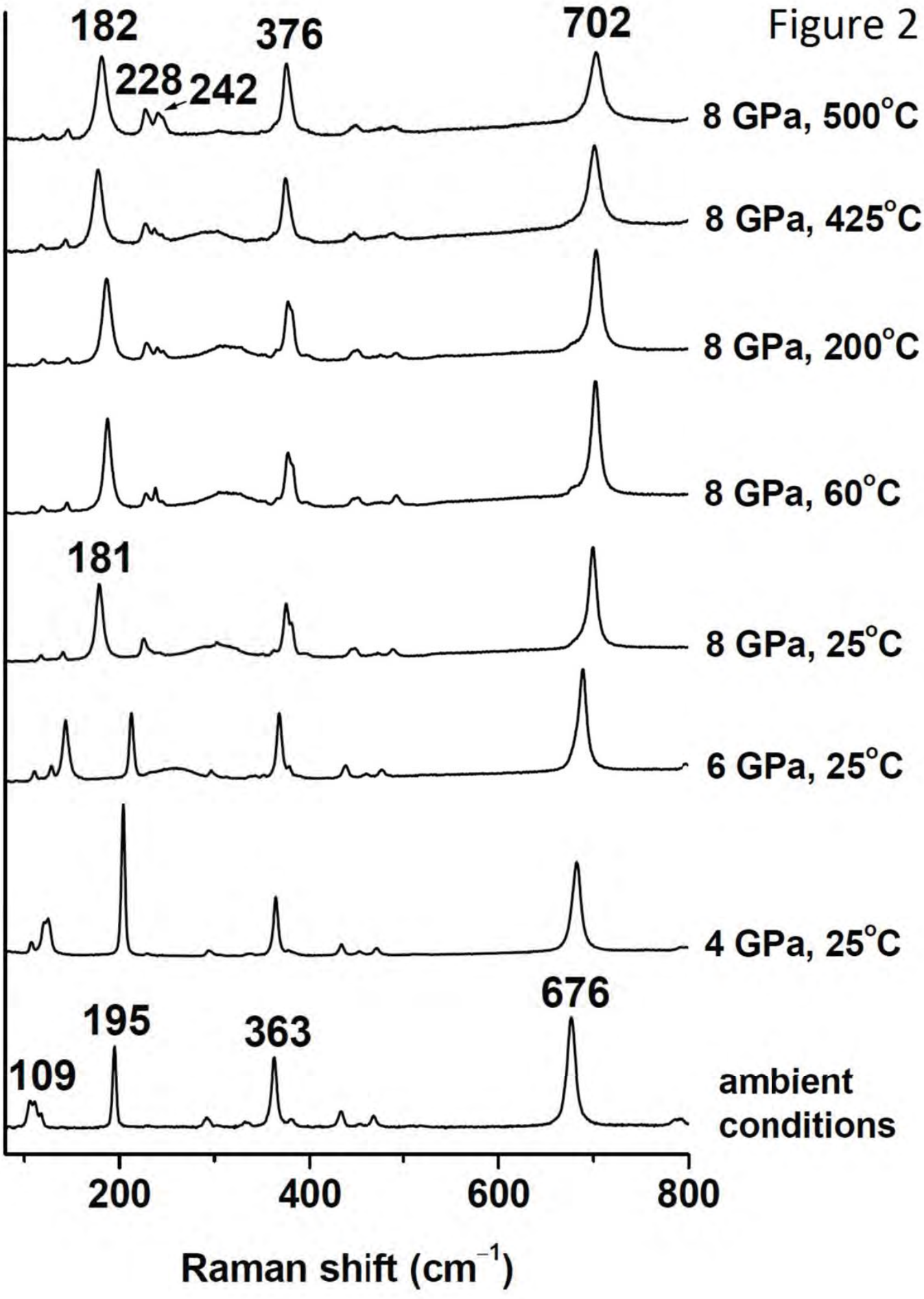
182
228
242
376
702
8 GPa, 500°C
8 GPa, 425°C
8 GPa, 200°C
8 GPa, 60°C
181
8 GPa, 25°C
6 GPa, 25°C
4 GPa, 25°C
676
195
363
109
ambient conditions
200
400
600
800
Raman shift (cm⁻¹)

Figure 3

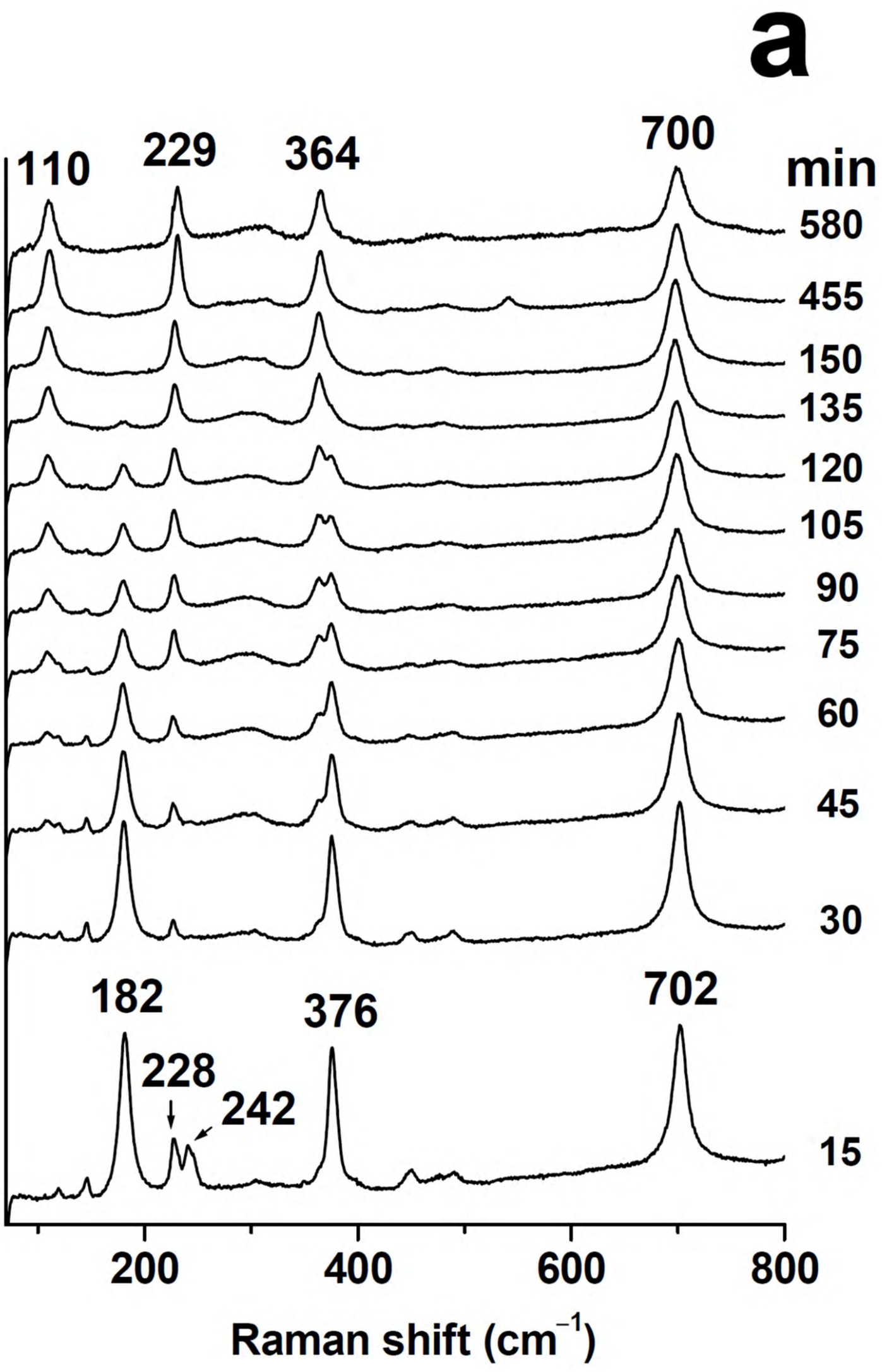
a
110
229
364
700
min
580
455
150
135
120
105
90
75
60
45
30
182
228
242
376
702
15
200
400
600
800
Raman shift (cm^{-1})

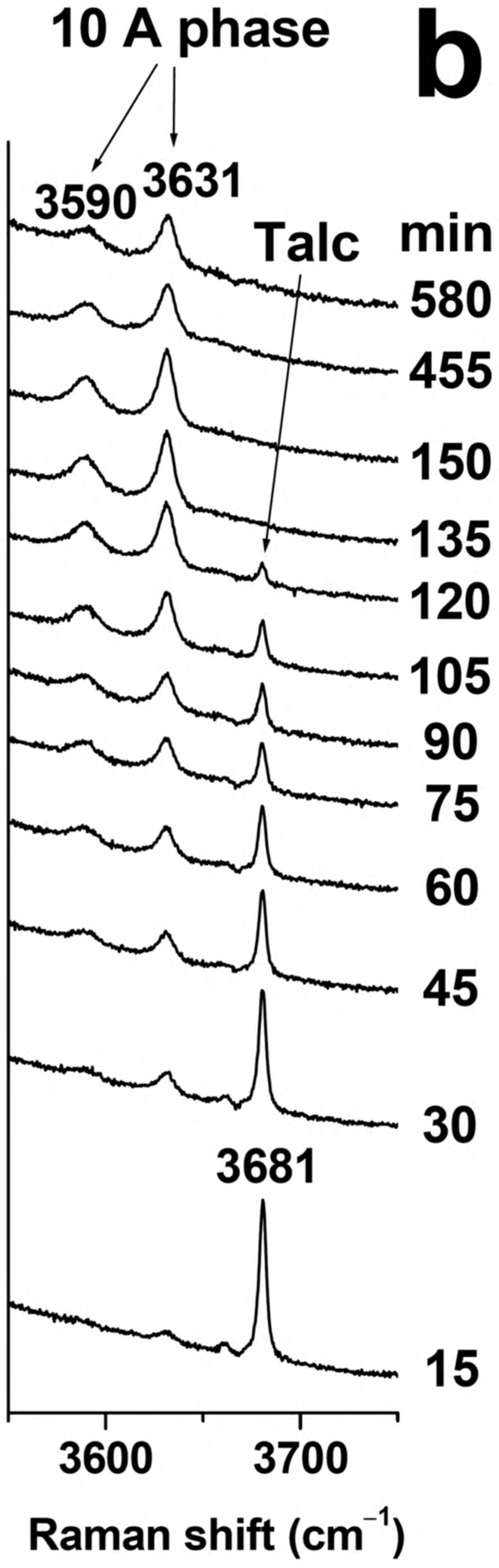
10 A phase
b
3590
3631
Talc
min
580
455
150
135
120
105
90
75
60
45
30
3681
15
3600
3700
Raman shift (cm^{-1})

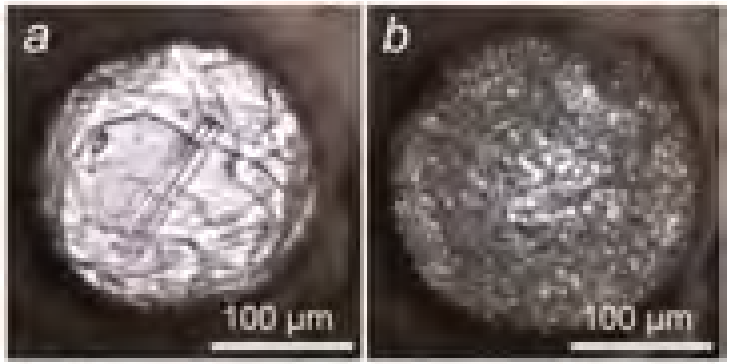

Figure 4

Figure 5

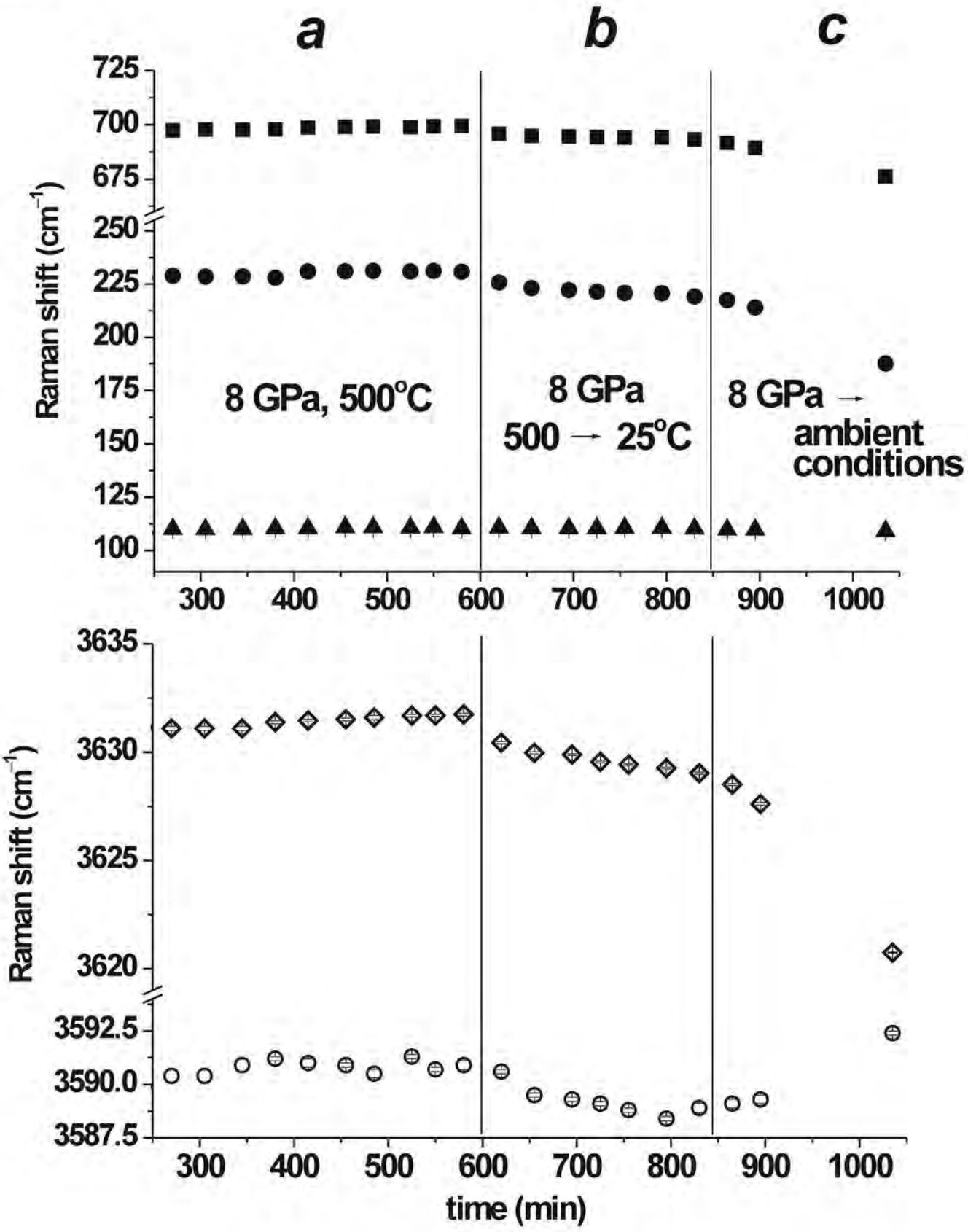
a
b
c
Raman shift (cm^{-1})
8 GPa, 500°C
8 GPa
500 → 25°C
8 GPa →
ambient
conditions
time (min)

Figure 6

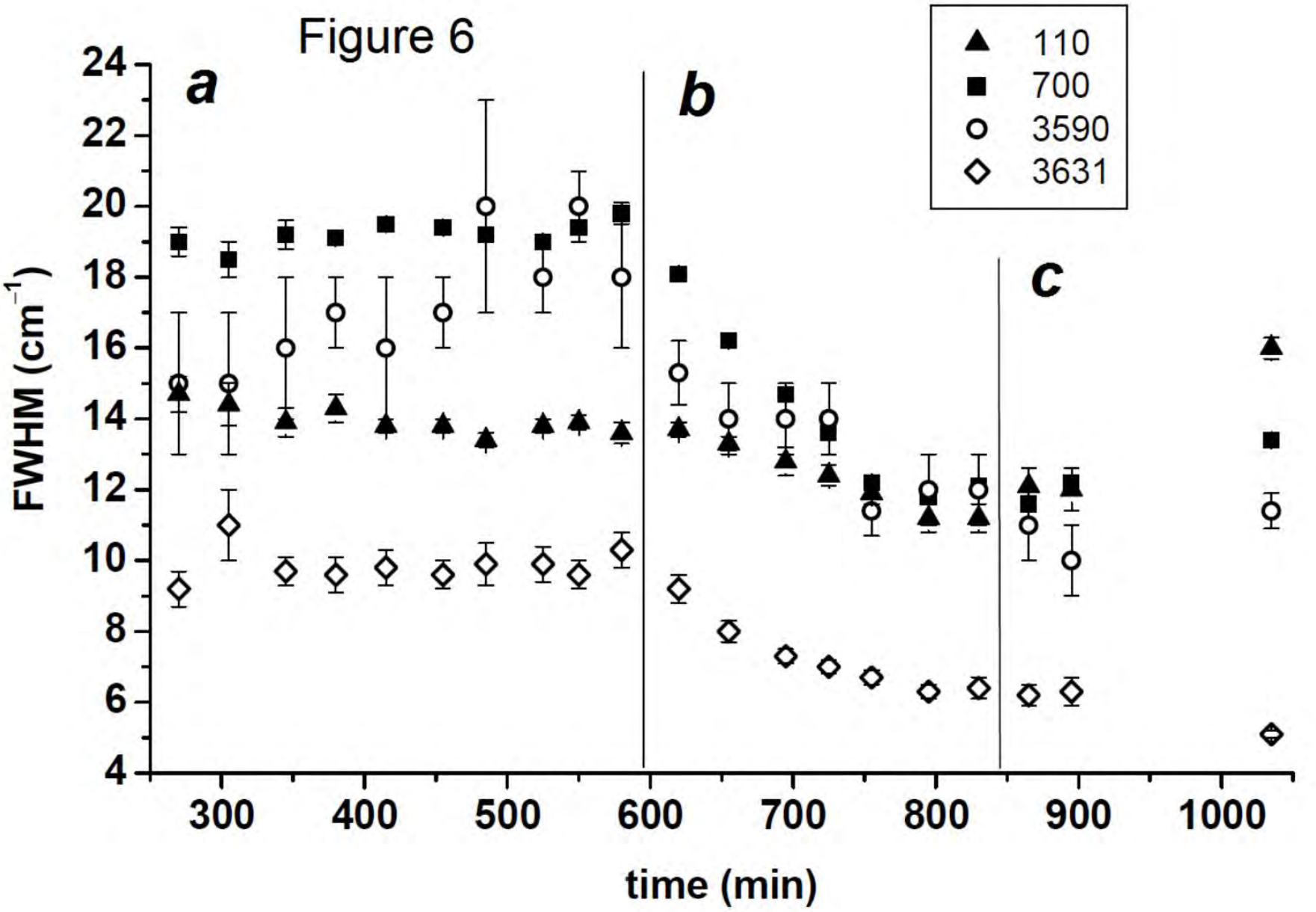
a
b
c
110
700
3590
3631
FWHM (cm^{-1})
time (min)
24
22
20
18
16
14
12
10
8
6
4
300
400
500
600
700
800
900
1000

Figure 7

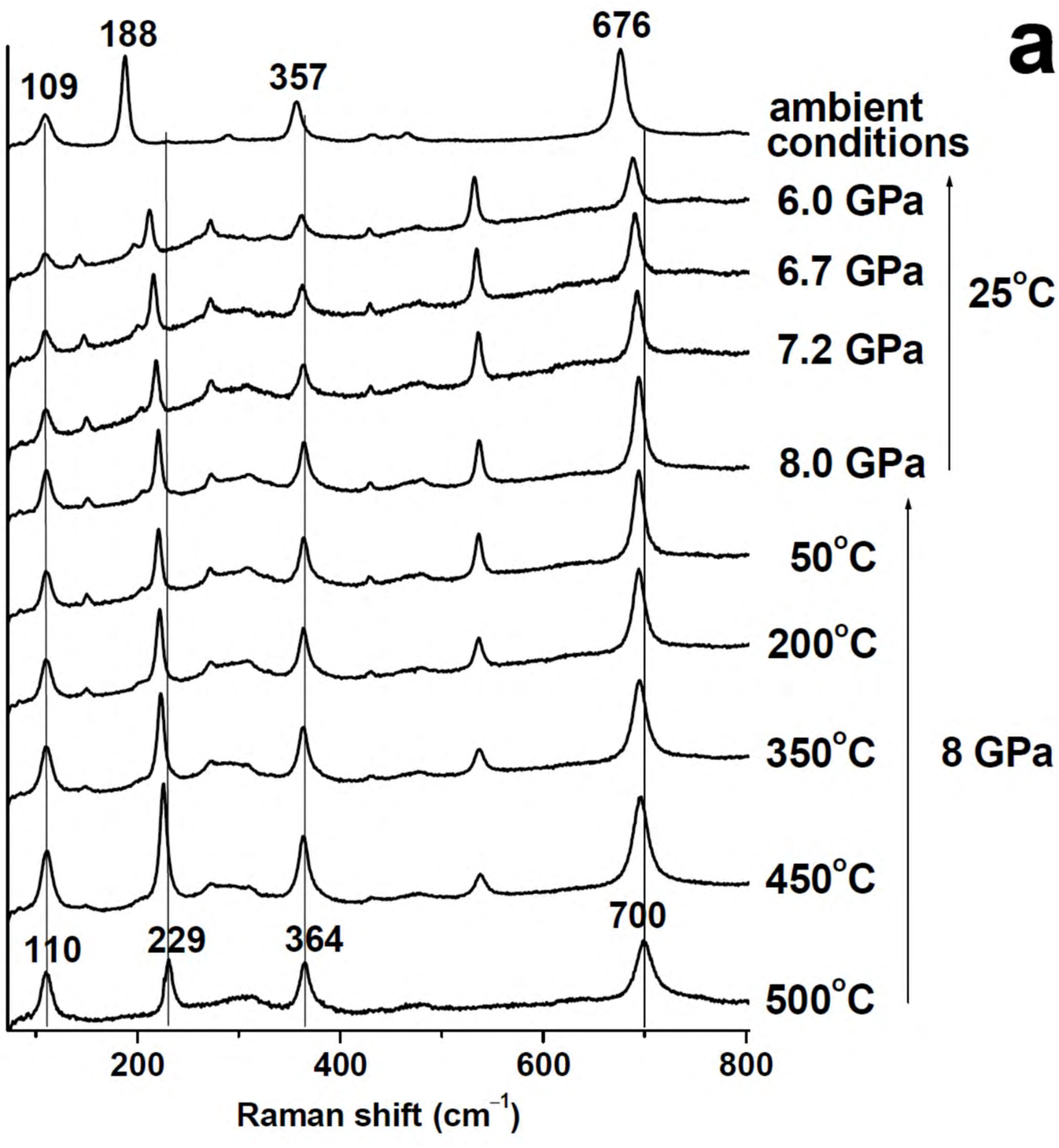
a
109
188
357
676
ambient conditions
6.0 GPa
6.7 GPa
7.2 GPa
8.0 GPa
50°C
200°C
350°C
450°C
500°C
25°C
8 GPa
110
229
364
700
200
400
600
800
Raman shift (cm⁻¹)

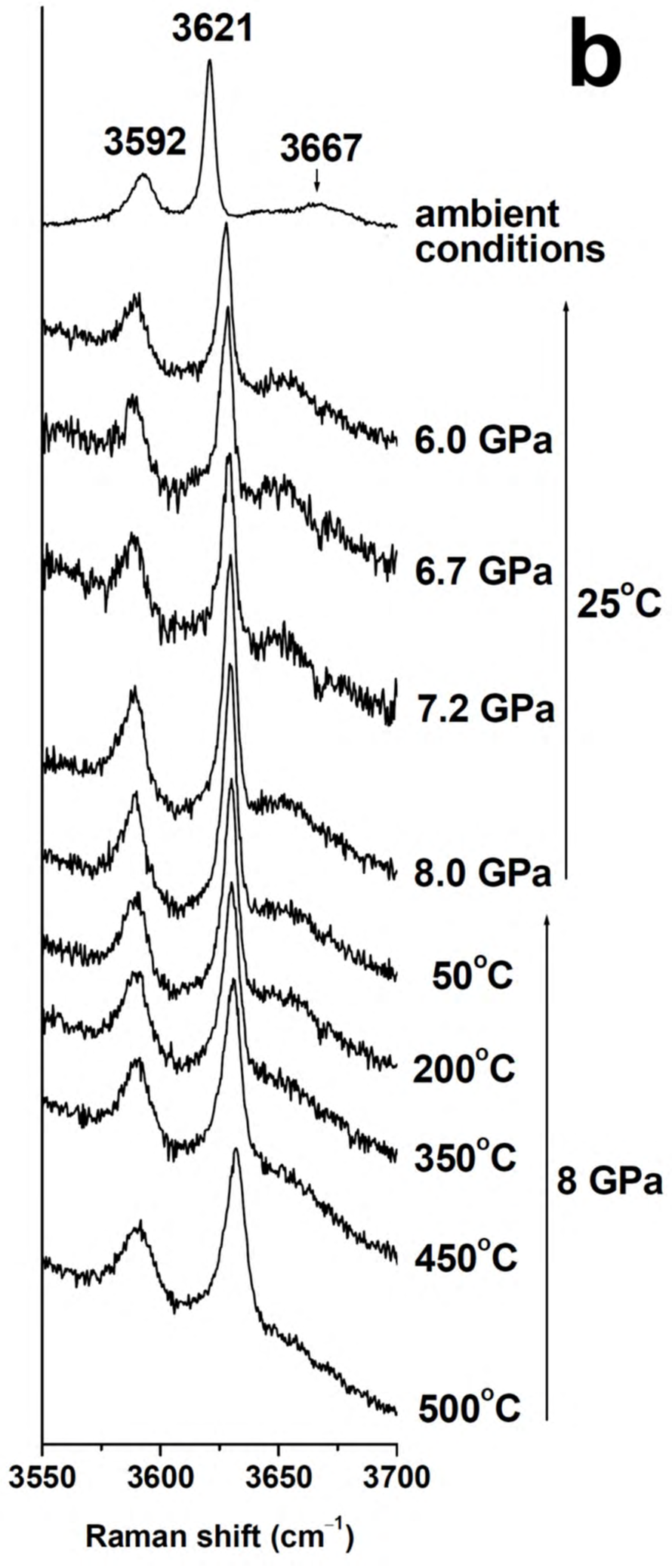
b
3621
3592
3667
ambient conditions
6.0 GPa
6.7 GPa
7.2 GPa
8.0 GPa
50°C
200°C
350°C
450°C
500°C
25°C
8 GPa
3550
3600
3650
3700
Raman shift (cm⁻¹)

Table 1. Raman bands (cm^{-1}) of talc and 10 Å phase. Band assignments are given according to the Raman study of talc (Rosasco & Blaha, 1980); the most intence bands are marked with asterisks.

Talc		10 Å phase				Band assignment
0 GPa, 25°C	8 GPa, 500°C	8 GPa, 500°C	0 GPa, 25°C	dν/dP (cm^{-1}/GPa) at 500°C	dν/dT (cm^{-1}/°C) at 8 GPa	
109*		110*	109*	0.17	0.000	MgOH
	119					
	146					
	182*					
195*	228*	229*	188*	4.14	0.016	MgOH
	242*					
292			289			
363*	376*	364*	357*			
433	449	434	432			Si-O-Si bending
452	476		451			
469	490	479	466			MgOH
		542				
676*	702*	700*	676*	2.24	0.007	Si-O-Si bending
790	811	817	785			
1017	1030	1034	1000			Si-O-Si symmetric stretching
1052	1050	1094	1058			Si-O stretching
		3590*	3592*	–0.49	0.004	OH stretching of interlayer H_2O
		3631*	3621*	1.07	0.004	OH stretching of interlayer H_2O
			3646			
3677*	3681*		3667			OH stretching of structural hydroxyls